Nanoscale

PAPER

View Article Online
View Journal | View Issue

Cite this: *Nanoscale*, 2025, **17**, 16523

Insight into charged drug release from metal–organic frameworks†

Josh Phipps,[a] Luis Pinzon-Hererra,[b] Wenlu Fan,[a] Sharmila Neupane,[a] Paige Walsh,[a] Abby Tian,[a] Teddy Biggin,[a] Jorge Almodovar,[b] Thamraa AlShahrani[c] and Shengqian Ma*[a]

The use of metal–organic frameworks (MOFs) as platforms in biological settings is an area in which they should shine, however, the adaptation of these materials in critical roles such as for drug delivery has been slow and limited. This can be attributed to the relative novelty of MOFs in the field and the lack of a comprehensive understanding surrounding how MOF components and solution conditions may influence release. In this work, we deliver broad view of how charged molecules are influenced by surrounding interactions to inform and improve drug release applications. To do this, a variety of MOFs [MIL-100, UiO-66, UiO-66-NH_2, UiO-66-NO_2, and UiO-66-OH] were synthesized to evaluate how the presence of functional groups and other electrostatic groups, like buffer molecules, ions, and polyelectrolytes, may influence loading and release of charged dye and drug models. To evaluate these results, we utilize the conventional Korsmeyer–Peppas (K–P) model which can inform us of the mechanisms of release. However, this and other models fail to adequately describe some of the biphasic release profiles observed. To overcome this hurdle, we present a novel adaptation of the K–P model by combining it with a burst release term while accounting for the proportion of release during each phase to describe the biphasic release observed. This allows for the extraction of empirical insights and the appropriate description of the mechanisms of release that would otherwise go unnoticed. In doing so, we reveal several phenomena present during release that can be used to better understand the process and can be leveraged to promote the controlled drug release of charged drug molecules.

Received 3rd April 2025,
Accepted 6th June 2025

DOI: 10.1039/d5nr01357g

rsc.li/nanoscale

Introduction

Metal–organic frameworks, with their porous nature, repeating subunits, and robust structure have shown great promise in a wide range of applications.[1] Their ability to be functionalized and vacant interiors make them excellent structures for sensing, separations, gas storage, and catalysis.[2–4] These same characteristics make them excellent platforms for use in biological settings as well through the isolation catalytic enzymes under adverse conditions,[5–10] as storage devices protecting housed chemicals or proteins from degradation,[11–13] and as delivery vehicles for the transport of drugs in therapeutics.[14–20] The large library of MOF linkers and node combinations available for selection allows researchers a unique ability and advantage over other platforms to create tailor-made MOFs for specific applications.[19,21,22] This has opened the door for creating delivery vehicles that can respond to environmental factors to trigger release where a burst release of drug is often achieved through the breakdown of the MOF structure.[22–26] Alternatively, robust components can also be selected that will allow the MOF to remain in its crystalline state to create a controlled release profile as the drug exits.[16,27–29] However, this boutique selection process can be arduous, costly, and yield mixed results leading to the slow adaptation of MOFs in the medicinal setting.[30] To overcome these challenges, a better understanding of drug-MOF interactions is necessary to usher in and streamline the implementation of MOFs for drug delivery.

Many studies have provided in-depth reports on the release of drugs in solution.[31–37] However, these typically focus on a particular drug for a specific application. This has led to a lack of a broad understanding on drug release, which has made it difficult to predict and select MOF components that will encourage the desired release profile of a given drug. This is further compounded by drug complexity. However, most drugs carry an inherent charge, either positive or negative, which can

[a]*Department of Chemistry, University of North Texas, Denton, Texas 76205, USA. E-mail: shengqian.ma@unt.edu*
[b]*Department of Chemical, Biochemical, and Environmental Engineering, University of Maryland Baltimore County, Baltimore, Maryland, 21250, USA*
[c]*Department of Physics, College of Science, Princess Nourah bint Abdulrahman University, Riyadh 11564, Saudi Arabia*

†Electronic supplementary information (ESI) available. See DOI: https://doi.org/10.1039/d5nr01357g

have a significant impact on how it interacts with its surroundings and has so far been an aspect of drug release that has not been adequately explored and may still house some key secrets.

To better understand how charged drug molecules may interact and be influenced by the surrounding MOF, methyl orange (MO) and methylene blue (MB) were selected to serve as drug models. These, along with their drug counterparts of epinephrine (Ep) and penicillin G (Pg) were selected for analysis due to their similarity in charge, with each bearing a single positive or negative charge, hydrophilic nature, small size, and the presence of aromatic groups. The resemblance in structural characteristics enable the evaluation of guest–host electrostatic interactions including possible hydrogen-bonding, dipole interactions, and π–π stacking while the small size of each allows the molecules to easily pass through the MOF pores with similar diffusion rates which can be evaluated through UV absorption *via* their aromatics. In order to provide a clear understanding of how electrostatic interactions may influence release, we probe a range of conditions including: loading amount, buffer concentration, presence of functional groups with electrostatic potential, and the presence of polyelectrolytes. To extract empirical data from these release studies, the Korsmeyer–Peppas model was selected to fit the release profile of each trial for its ability to provide empirical data and reveal mechanistic insights during release.[38] However, this, like many other mathematical models, does not adequately fit biphasic release profiles. To rectify this, we adapted the model to create a novel mathematical model that appropriately describes the biphasic release of molecules from MOFs while retaining key terms providing the ability to reveal mechanistic insights.

Inspired by the results from MO and MB testing, we expanded our analysis to evaluate the release of epinephrine and penicillin, two oppositely charged drugs that are commonly used to treat the life-threatening conditions of anaphylaxis shock and bacterial infections, respectively. Both drugs share a similarity in that they suffer a deleterious susceptibility to oxidative degradation which makes extension of their longevity and shelf-life an important medical concern.[39,40] Furthermore, these conditions require a timely administration to have their desired effect, making the two drugs excellent candidates as representative samples for testing.

In this work, we seek to provide a more clear and broader view of how charged molecules are affected by the pore environment of MOFs and how the release profiles can be selected and improved. To do this, we identified and synthesized a variety of MOFs to probe the effect of environment and the presence of functional groups and other electrostatic groups that may affect the loading and release kinetics of charged molecules (MO/MB) as well as a proof-of-concept test using epinephrine and penicillin. We also created a novel adaptation of an existing mathematical model to appropriately fit and extract empirical insight from biphasic release profiles. In doing so, we reveal several phenomena present within of the pores of MOFs that can be leveraged to promote controlled drug release of charged drug molecules.

Experimental

MOF synthesis

All MOFs were synthesized and characterized according to reported procedures with minor modifications. The detailed synthesis of each MOF and chemicals used can be found in the ESI.† [41,42]

Dye loading

Stock solutions of methyl orange (MO) and methylene blue (MB) were created by dissolving solid dye in deionized water until the solutions were saturated. The solutions were then centrifuged to remove any excess solid and their concentration was determined *via* UV-visible spectrometry using their molar absorptivity and absorption at 465 and 665 nm, respectively. Following this, two experimental loading conditions were created, one for each dye, to observe the loading of dye into MIL-100(Fe). The final solution had a volume of 1 mL and was composed of 5 mM dye (MB/MO), and 50 mg mL^{-1} MIL-100 (Fe). After this test, standard conditions were selected, and loading continued for each MOF type. These solutions were created in triplicate with each composed of 4 mM dye (MB/MO), 20 mM pH 7 HEPES buffer, 1 mg mL^{-1} of each MOF, and with a total volume of 0.5 mL. These tubes were then lightly vortexed and allowed to sit for 7 days in the dark at 4 °C. After this period, aliquots of supernatant were extracted and diluted to either 1 mL for MO, or 3 mL for MB. Absorbance was then measured using UV-Vis against a ladder to determine the amount of dye loaded.

Drug loading

Epinephrine and penicillin were independently loaded in five separate solutions each combining the drug (1 mg mL^{-1}) and MIL-100(Fe) (1 mg mL^{-1}) in DMSO solution with a final volume of 0.5 mL. The mixtures were lightly vortexed and allowed to sit covered in the dark at room temperature for 7 days. At the end of 7 days, samples were centrifuged for 3 minutes at 6000 rpm and the supernatant was removed. Aliquots of the supernatant were then measured with UV-Vis to determine loading with loading reported as the mean.

Dye release

To isolate the loaded MOF samples, excess solution was removed from loading solutions until the total volume was 300 μL. Next, the solution was mixed thoroughly by pipette and 100 μL of the solution was removed and placed into a new microcentrifuge tube. The tube was then centrifuged for 3 minutes at 6000 rpm and the liquid was removed, leaving the MOF pellet. This process was repeated two more times to give three samples of equivalent loading and mass.

For each sample, release was conducted following these standard conditions unless otherwise specified. Here, 1 mL of 20 mM HEPES buffer at pH 7 was added to the microcentrifuge tube and quickly vortexed to mix. An aliquot of the solutions was then removed and added to a UV cuvette with 20 mM pH 7 HEPES buffer. The solution was briefly inverted,

and then inserted into the UV-Vis for a time-course measurement. The cuvette was removed and inverted at 30 seconds intervals for the first 5 minutes, then at 1 minute intervals until a final time of 10 minutes was reached. Release was completed in triplicate for each condition with values were reported as means.

Drug release

The same isolation protocol for the dye loaded MOFs from above was repeated until MOF samples were recovered. The MOF samples were then individually suspended in 1 mL PBS solutions of either 0.1% or 1% by weight PEI. The solutions were gently vortexed and allowed to sit for 5 minutes. After this, the samples were immediately centrifuged at 13 000 rpm for 5 minutes and the supernatant was removed for testing against concentration ladders using UV-Vis. This process was completed in triplicate for each condition with values reported as means.

Cell studies

Details regarding cell studies can be found in the ESI.†

Results and discussion

In order to evaluate how charged drugs are affected by pore environment, MIL-100 was selected as a standard for analysis for its biocompatible nature, cage type pores (2.5–2.9 nm), and small pore window (0.55–0.86 nm) which would necessitate the passage of the models through these smaller spaces, thereby inherently controlling release.[42–44] Alongside this, a series of UiO MOFs including UiO-66 and its derivatives functionalized with amine, nitro, and hydroxyl groups were selected to create variations in the electrostatic environment within MOF pores of smaller size (0.8–1.1 nm), but similarly sized pore windows (0.6 nm). These Zirconium-based MOFs provide a facile synthesis and robust structure which ensures consistent pore size and shape between each group. Additionally, this smaller pore size increases the influence of the functional groups present and allows for superior comparisons to be made between each group. Each MOF was successfully synthesized and characterized using powder X-ray diffraction (PXRD), Brunauer–Emmett–Teller (BET) analysis, thermogravimetric analysis (TGA), particle size analysis, zeta potential, and scanning electron microscope (SEM) (Fig. S5–S11†). The obtained data was consistent with previous reports.[41,42] Together, these MOFs will allow for the evaluation of the release rate of the charged models as variations in the pore are adjusted (all fitted plots can be found in the ESI, Fig. S12–S23†).

MOF loading

As an initial test to determine loading, buffer condition for release, the uptake of both dyes into the MOF was observed after 7 days. As there was nearly complete loading for both models, with 98.6% loading observed for MO and 100% for MB, no significant variations in loading could be observed. Following this, the loading conditions were adjusted as described above to create standard conditions for the subsequent tests. During this loading some key differences between each MOF were observed that are quite telling (Fig. 1).

First, the loading for MO among each MOF was consistently higher than that of MB, which is not surprising as the negatively charged dye is expected to coordinate to the positive metal sites within the framework, while the positive dye would either not interact or be slightly repelled. This was evident through IR spectroscopy where when MO was present a red shift of a diagnostic in-plane C–H bending mode from 1043 to 1030 cm^{-1} was observed. It is worth mentioning that this mode has been shown to be quite sensitive to its local environment.[45,46] This observed shift is a result of a decrease in bending deformation energy arising from increased attraction between the metal center and the dye and illustrates how closely coordinated the negatively charged dye is to the metal center (Fig. 2). In contrast, when MB was present the same feature shifted only 3 cm^{-1}, indicating a far weaker interaction between the positively charged dye and the MOF metal centers. Mechanistically, these differences in interactions would implicate the negative charge present on the MO in hin-

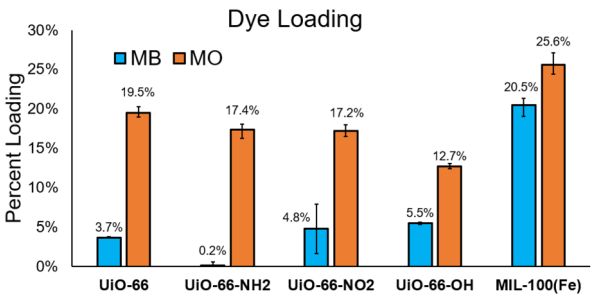

Fig. 1 Percent loading of MB and MO in each synthesized MOF. Results are shown as mean ± standard error of the mean (n = 3).

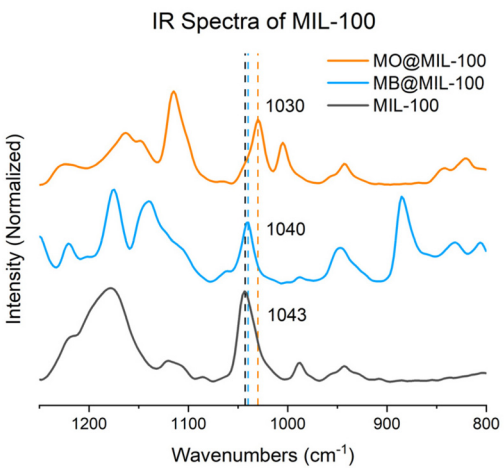

Fig. 2 Plot of IR spectra gained from the loading of charged dyes into MIL-100.

dering the release of the molecule from within the MOF pore, while the MB would more readily escape. Additionally, the strong interaction with the metal center suggests that the MO interacts more closely with the MOF at the pore interface, allowing for much of the pore window to be utilized upon release. In contrast, the decreased interaction or possible repulsion by the metal center with the MB dye at this interface likely leads to a shrinking of the pore window available for passage of the molecule.

The next key finding observed was that the presence of functional groups plays a significant role in the loading of charged molecules. The partial charges present among the nitro and hydroxy functionalized UiO-66 showed very little variance with only a slight decrease in loading compared to the unfunctionalized control for the MO, attributable to the increased steric effects from the functional groups. Conversely, there was an increase for MB loading, which can be attributed to the partial positive charge present. Similarly, there was clear divergence between MO and MB in the amino functionalized MOF compared to the others with a loading of 17.4% and only 0.2% respectively. This strongly indicates that the partial positive charges among this functional group takes part in electrostatically repelling and preventing the similarly charged MB from entering or persisting in the pore, creating an undesirable environment for the model. We also observed a slight increase in loading for the MIL-100, which achieved a loading of 25.6% MO and 20.5% MB. This increase is expected as the available pore space for MIL-100 is larger than that of the UiO MOFs allowing our dye models greater inhabitable space within the pore (Fig. S3†).

Finally, we loaded MIL-100 with the biologically relevant positively charged epinephrine (Ep) and the negatively charged penicillin G (Pg). These loadings showed a marked increase in loading compared to the dyes with final loadings of 45.3% (453 μg mg^{-1} MOF) and 60.5% (605 μg mg^{-1} MOF) respectively (Fig. 3). For relevance, if full release is achieved, 1 mg of MOF would supply a higher dose than that of a standard EpiPen which typically contain 300 μg per dosage.

The higher loading observed compared to the dye models can be attributed to the presence of DMSO rather than water during the loading which has lower polarity and thus, weaker hydrogen bonding interactions allowing the drugs to diffuse into the MOF pore with less hindrance. This solvent was selected due to the poor solubility of each drug in water at physiological pH, ability to protect each drug from oxidation due to the removal of water, and for its biocompatibility at low concentrations.

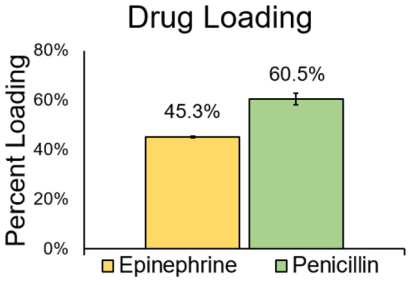

Fig. 3 Percent loading of drug models within MOF MIL-100. Results are shown as mean ± standard error of the mean (n = 3).

Mathematical models for empirical insights

To extract empirical insights from the release data and to further support conclusions, the Korsmeyer–Peppas (K–P) model was utilized, denoted below as eqn (1) (plots can be found in ESI on pages S12–S23†)

$$\frac{M_t}{M_\infty} = k \cdot t^n \tag{1}$$

where M_t represents the amount of drug released at time t, M_∞ is the total releasable amount of drug, k represents the release rate constant with units of min^{-n}, and n is the release exponent which is dimensionless and can inform the mechanism of release.[38,47] Together, this model provides us with mechanistic insight into the release of drugs from materials and can aid in describing the release type. These types of release include Fickian diffusion, where release is controlled by diffusion alone. This is indicated by a value of n = 0.43 for spherical models, which most closely resemble the selected MOFs. Next, is anomalous transport, where a combination of diffusion and other interactions take place ($0.43 < n < 1$). Zero-order release is observed when $n \approx 1$. In this type, the rate of release is controlled by something independent of concentration gradients and is characterized by the rate being linear with time. A value of n being less than 0.43 would indicate a resistance to diffusion and interactions between the dye molecules and its surroundings. In regard to k, this value represents the rate at which release takes place and can inform of the systems' speed of release. When combined, this model can provide a good picture of factors influencing release rather than evaluating the rate alone.

However, this model fails to adequately fit the release profile when burst release is observed. While other models have been used in the past to fit burst release profiles, the mechanistic insight brought by the K–P model is often lost. Because of this, the K–P model was adapted to appropriately fit these biphasic release systems into a new equation below which, to our knowledge, has not previously been reported.

$$M_t = M_\infty \cdot [A(1 - e^{-k_1 t^{n_1}})] + B k_2 t^{n_2} \tag{2}$$

In this equation we combine the power-law diffusion phase term from the K–P model ($k_2 t^{n_2}$) with a general burst release exponential term ($1 - e^{-k_1 t^{n_1}}$) similar to that of the Weibull model that complements the model by allowing for the description of the cumulative release of a molecule from a biphasic system.[48,49] Here, similar to the K–P model, k_1 is the burst phase rate constant, however, in this equation, n_1 adjusts the time dependence of the burst release, but is still related to release profile where if $n_1 \approx 1$ the release follows exponential burst release, while if $n_1 < 1$, it implies that the release initially

occurs quickly and decelerates over time. This represents a decrease in the molecules that are readily available for release as time continues and further indicates that there are interactions preventing free diffusion. Similarly, if $n_1 > 1$ a sigmoidal curve would be observed indicating that there is an initial barrier that must be overcome before the full potential of the release rate is achieved. The most common example of this would be due to the addition of coatings surrounding the MOF.

Here, we define $A + B = 1$ where both are dimensionless and A is a value between 0 and 1 representing the fraction of molecule released during the observed burst phase and $B = 1 - A$ representing the fraction responsible for the diffusion phase observed after the initial burst release. Finally, following standard practices in release kinetics, we calculated time at which 95% completion of the burst phase occurred using eqn (3) below.

$$t_{95\%} = \left(\frac{2.995}{k_1}\right)^{\frac{1}{n_1}} \quad (3)$$

This equation is commonly used identify the threshold where the crossover of the two release types occurs. Together, these calculations were used to plot the fitted results to our data with an R^2 within acceptable ranges for each plot (0.99–0.82), indicating a good fit and reliable results. Compared to the K–P model, our biphasic model provided a superior fit to our biphasic data and revealed further empirical information that would have otherwise gone unnoticed.

Effect of buffer on charged dye release

After completion of loading tests, the release of MO and MB from the lightly loaded initial samples of MIL-100 were selected for evaluating the effect of buffer concentration on release rates. These were selected as the lower concentration and lack of buffer during loading would emphasize the differences among results. The release profiles were observed in HEPES buffer at pH 7 with increasing concentration of 0, 20, 50, and 100 mM.

For the positively charged MB dye, during release we observed a slow and measured first order release with no added buffer present (Fig. 4a). When using eqn (1), it was clear that this release was dominated by diffusion as its n had a value of 0.51. Additionally, the slow rate of diffusion was reflected in the k value of 0.008 (Table 1). However, as the concentration was increased to 20 mM and 50 mM, we observed a marked increase release rate with a burst release taking place where the rate increased by approximately 8 and 15 times, respectively. However, instead of continuing to full release, the rate of both trials plateaued and continued their release over time. This was reflected in the proportion released where 18.1% was released in the 20 mM trial and 35.0% in the 50 mM trial after the allotted time (Table S2†). This increased rate is understood to be due to the inclusion of similarly charged Na^+ counter ions present that accompanied the HEPES buffer.

Due to the Biphasic release profile, eqn (2) was utilized for these tests. The results indicate that the 20 mM trial had an initial burst release that followed the exponential trend well with a n_1 of 0.91 and a k_1 of 1.803. This was followed by typical Fickian diffusion demonstrated by a n_2 of 0.45 and a k_1 of 0.033. For the 50 mM trial a more intense burst result was observed with a n_1 of 0.93 and a k_1 1.418. However, the diffusion phase of this trial showed a significant decrease in rate where k_2 was 0.005 and n_2 had a value of 1.00. This result coupled with the lack of full release (~65% remaining) suggests that after the initial burst release, the higher concentration of buffer leads to crowding and competition of

Table 1 k and n values calculated using eqn (1) and (2) during buffer release testing with k_1 and n_1 values in gray, and k_2 and n_2 values in black

	MO		MB	
Buffer concentration (mM)	k	n	k	n
0 mM	0.022	0.64	0.008	0.51
20 mM	0.021	0.73	1.803	0.97
			0.033	0.45
50 mM	0.030	0.72	1.418	0.93
			0.005	1.00
100 mM	0.032	0.68	0.053	0.52

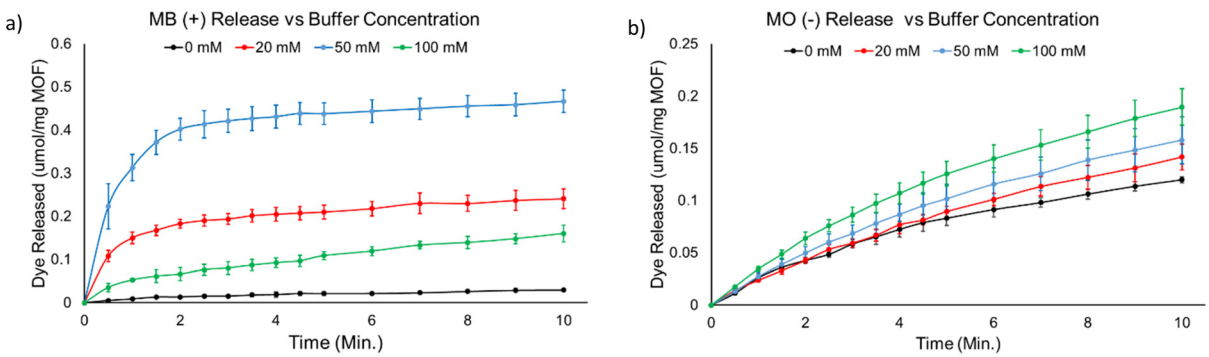

Fig. 4 Release profiles of MB (a) and MO (b) from the lightly loaded MOF MIL-100 as buffer concentration is increased. Data are shown as mean ± standard error of the mean (n = 3).

diffusion at the pore window of cages within the MOF in agreement with our earlier prediction. Here the relatively high concentration of buffer meets the lower concentration of dye and the diffusing force of the dye is overcome, hindering its release and resulting in the slower release rate which remains promoted as indicated by the n_2 at 1.

This trend is carried forward as the buffer concentration is increased to 100 mM. Here, there was a precipitous decline in the release rate to roughly 5 times that of the buffer free solution with only 12.0% of the dye escaping. This was accompanied by a lower k of 0.035 and a n value of 0.52 indicating slow assisted release. This slower rate is likely due to the same congestion effect at the pore window interface observed during the 50 mM trial, however, instead of occurring further within the MOF, this result indicates that the crowding occurs closer to the periphery.

The inclusion of buffer within the solution leading to an increase in the release has been reported before and is consistent to a previous report by Rosi and coworkers.[50] In the study, the presence of ions in solution was shown to trigger the release of loaded material from MOFs by disrupting the ionic interactions between a loaded drug and the surrounding framework. The same trend is observed here as there is a weak interaction between the dye and the framework (Fig. 2), however, the release is more likely due to the repulsive force of the ions infiltrating the pore where the dye is present. Additionally, there appears to also be a concentration dependence in regard to release rate and that this rate can be limited by increased concentration.

When MO loaded MIL-100 was exposed to the same conditions, it was observed that that there were only slight variations in its release rate as buffer concentration was increased from 0, 20, 50, to 100 mM with all results showing a measured release with first order kinetics that was directly related to buffer concentration (Fig. 4b) with likewise results for percent release of 9.6%, 11.3%, 12.6%, and 15.1% respectively (Table S2†). This is the result of the electrostatic interactions present where the negatively charged dye strongly interacts with the MOF and must be displaced by a strong enough diffusion force or the competition of similarly charged moieties (Fig. 2). The IR spectra for both dyes support this and indicate that the positively charged MB resides within the pores of the MOF with weak interactions and is forced out, not only by diffusion but is also influenced by the presence of the buffer components (*i.e.* Na^+ ions). This is a realistic outcome as the partially negative HEPES likely coordinates to the MOF in the same manner as MO, while the positive Na^+ ions would have a similar repelling effect to that of the amine group present on UiO-66-NH_2 observed during the loading testing. Additionally, there was no observed limitation to release rate corresponding to buffer concentration as observed in the MB trials, further supporting our position that the negatively charged dye has increased access and/or experiences less congestion at the pore window interface. Together, these results show that charge is an essential factor to consider when selecting conditions for release and that this process can become hindered as concentration of other solutes increases in the release medium.

Effect of loading on charged dye release

After adjusting loading to standard conditions, we compared the release profiles of the two loading conditions from the MOF MIL-100. When comparing the uptake, we see an increase from 0.094 μmol per mg of MOF to 1.06 for the MO trial and a similar increase from 0.1 μmol per mg of MOF to 0.89 for MB. This significant increase results in surprisingly very little change in the proportion of release for MB with the release from the lightly loaded sample reaching 18.1% release over the course of the 10 minute trial, while the release from the standard loaded sample was 17.8% (Fig. 5 and Table S2†) indicating that the absence of buffer during the loading and subsequent introduction of an equivalent concentration to the lightly loaded trial did not appear to affect the release as time increased. There was, however, significant change in the shape and values calculated from eqn (1) and (2) (Table 2). While the lightly loaded sample showed a burst release profile, followed by typical diffusion (n_2 = 0.45), the standard loading condition followed a slow (k = 0.037) zero-order release profile, likely the result of the same crowding observed during the 100 mM release.

On the other hand, the MO release profiles appear to have the reverse trend occur when concentration increases. Here, the release profile for the lightly loaded trial showed zero-order release and the standard loaded yielded first-order release. When comparing the release rates, we observed that there was a direct correlation between the rate of release and the increased loading (k_{light} = 0.025, k_{Std} = 0.078) with the lightly loaded samples releasing 10.3% and the standard loaded samples releasing 25.4% over the same period. Additionally, when the lightly loaded MO is compared to the standard loaded MB, there are similar n values, indicating a similar mechanism of release where both are likely encountering congestion at the pore window. The results from this test further supports that there is a concentration dependent effect between the negatively charged dye concentration and release

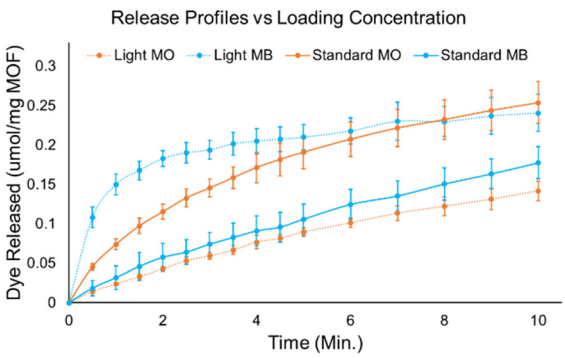

Fig. 5 Release profiles of dyes from the lightly loaded and standard loaded MOF MIL-100. Data are shown as mean ± standard error of the mean (n = 3).

Table 2 Loading condition results showing k and n values calculated using eqn (1) in white. Eqn (2) k_1 and n_1 values are shown in grey, and k_2 and n_2 values in black

	MO		MB	
Loading condition	k	n	k	n
Light	0.025	0.73	1.803	0.97
			0.033	0.45
Standard	0.078	0.51	0.037	0.73

Table 3 Results showing k and n values calculated for the release of dye from functionalized UiO-66 and its derivatives with results from eqn (1) in white. Eqn (2) k_1 and n_1 values are shown in gray, and k_2 and n_2 values in black

	MO		MB	
MOF	k	n	k	n
UiO-66	0.209	0.69	0.209	0.67
UiO-66-NH_2	0.217	0.26	0.091	0.97
	0.684	1.31		
	0.070	0.12		
UiO-66-NO_2	0.149	0.22	0.201	0.61
	0.754	0.74		
	0.002	0.00		
UiO-66-OH	0.085	0.76	0.064	0.39

rate where coordination slows release while the release rates for MB appear to be controlled instead by a steric competition at the pore window.

Effect of functional groups on charged dye release

To probe what effect common functional groups with electrostatic potential may have of the release of charged drug models, release trials of both dyes were performed from the synthesized UiO-66 variants using standard conditions described above. From the plots of these release trials, we can clearly see that the absence of functional groups results in a faster release rate regardless of model charge (Fig. 6). Notably, the K–P variables for the unfunctionalized MOF indicate a fast and similar mechanism of release anomalous transport for both models with k = 0.209 and similar n values of 0.69 for the MO and 0.67 for MB (Table 3). This indicates the UiO-66 likely has a balanced charge under these conditions.

When we compare the functionalized UiO-66 MOFs to this control, there is an interesting amount of variation among the results. In the MO plots, the amine and nitro functionalized MOFs appear to show a fast initial release, before the rate is slowed, which suggests that the loosely bound or free MO within the MOF is released quickly before the diffusion of the strongly coordinated dye takes place (Fig. 6a). This is supported by the K–P values which indicate that both appear to interact strongly with the negatively charged MO with n values of 0.26 for the amine and 0.22 for the nitro functional groups and show that the release is severely hindered. These interactions appear to have very little effect on the rate constant, however, with the amine functionalized MOF showing a slight increase in k from 0.209 for the bare MOF to 0.217, and the nitro functionalized MOF yielding a slight decrease to 0.149. When eqn (2) is applied to the release profiles of UiO-66-NO_2 and UiO-66-NH_2, further empirical data can be gained to support these conclusions with both showing an initial burst release of uncoordinated MO and a subsequent slow, heavily hindered diffusion release phase. However, the release of the MO from the nitro containing MOF nearly ceases all release indicating the stronger interaction with the negatively charged dye.

When MB is released, a weak force influencing the release when the nitro groups is present indicated by the n value of 0.61 and an increase in k to 0.201 (Fig. 6b). Similarly, a strong force is indicated by a n of 0.97 in the amine trial leading to zero-order release and a small k of 0.091, which can be attributed to the low loading (Fig. 1). These findings suggest that the partial positive charge found on the Nitrogen within the functional groups, effectively push the dye from the pore of the MOF through a repelling electrostatic interaction with the amine group having a stronger partial positive charge which in consistent with its observed positive zeta potential of 14.7 mV (Table S1†). This effect is supported by the trial with the

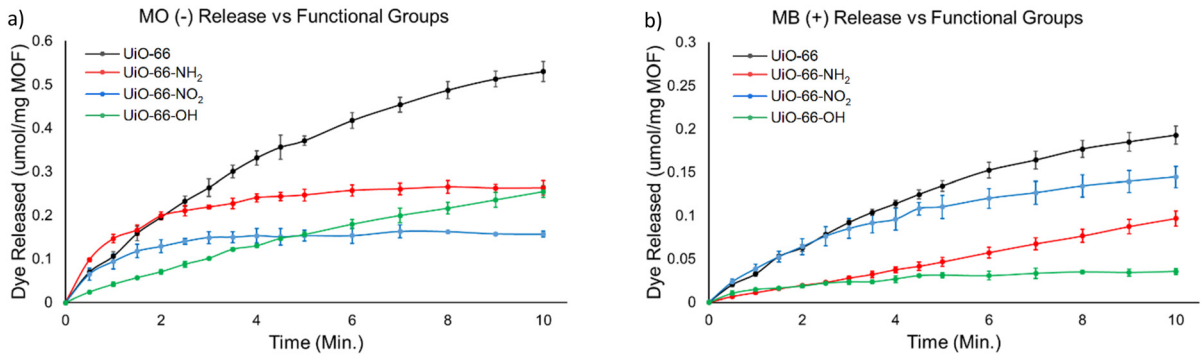

Fig. 6 Release plots showing the release of MO (a) and MB (b) from functionalized and non-functionalized UiO-66 variants. Data are shown as mean ± standard error of the mean (n = 3).

hydroxyl group where the partial negative charge among the Oxygen leads to the inverse of this trend with the n_{MO} showing an increase to 0.76 with a small k of 0.085 compared to the control and resulted in a zero-order release profile while the n_{MB} trial showed a decrease to 0.39 with a k value of 0.064. This change in n supports the presence of a force encouraging the transport of the MO out of the MOF, while the low k indicates there is a restricted speed of release for both models. This slow rate of release can be attributed to the increased presence and strength of hydrogen bonding between the model and the MOF within the pore. The combination of these findings suggests that there are push and pull electrostatic interactions taking place leading to a greater force required to allow the dye to escape the pore, but once free it is influenced by its surroundings. These results indicate that the presence and composition of the functional groups among the MOF are intricately related to the release rate and can be selected according to their electrostatic potential and ability to hydrogen bond allowing for the controlled release of charged molecules.

Effect of polyelectrolytes on charged dye release

After observing how significantly electrostatic effects influenced the rate of release of the charged dye molecules, the addition of polyelectrolytes to solutions was evaluated to determine if the effect could further be leveraged. To test this, the standard conditions using MIL-100 were replicated and the negatively charged polyelectrolyte Heparin (HEP), which has been used to coat the exterior of MOFs and the positively charged Polyethyleneimine (PEI) were introduced. This led to several notable outcomes.

When the release solution is composed of 0.1% by weight of HEP, the release for the MO loaded MOF followed the same first order release of the standard condition, but the release percent nearly doubled to 47.7% compared to 25.4% (Fig. 7 and Table S2†). This result is surprising as it is typically understood that the HEP and other negatively charged polyelectrolytes bind to the exterior of the MOF and effectively inhibit release. However, there appears to be little difference in the n values of both the standard and HEP trials with both rounding to 0.51 indicating anomalous transport (Table 4). However, the k for the HEP trial nearly doubled to 0.153 from 0.078 suggesting that while the mechanism for release does not change, there is an observed increase in release that is likely the result of greater competition for the coordination sites. Furthermore, the increased rate of release suggests that there is no inhibition of the release of the negatively charged dye and indicates that the HEP fails to coat the exterior of the MOF leaving the MOF pore windows open for release, at least during this time frame.

Table 4 Polyelectrolyte trial results showing k and n values calculated using eqn (1) in white. Eqn (2) k_1 and n_1 values are shown in gray, and k_2 and n_2 values in black

	MO		MB	
Condition	k	n	k	n
Standard	0.078	0.51	0.037	0.73
0.1% HEP	0.153	0.51	0.018	0.66
0.1% PEI	0.150	0.45	0.030	0.93
1.0% PEI	2.037	1.26	0.231	1.19
	0.035	1.00		

When release is monitored using the same concentration of positively charged PEI, a similar trend is observed where first order release continues, the percent release only slightly decreases to 40.6%, and values for n and k likewise decreased to 0.45 and 0.150, respectively. The similarity between these two polyelectrolyte groups suggests that the negatively charged polyelectrolytes compete quite similarly to the Cl^- ions and PEI. However, the PEI likely contributes to steric interference preventing a portion of the MO dye from escaping leading to the decreased n value and slightly poorer performance.

When we test the presence of polyelectrolytes on the release of MB, the first notable difference is that each trial resulted in zero-order release profiles (Fig. 7b). The next key finding is that, unlike in the MO trial, the presence of 0.1% HEP results in is a sharp decline in release where there is only 0.08% released after 10 minutes compared to the 17.8% observed under standard conditions. This follows expected outcomes as

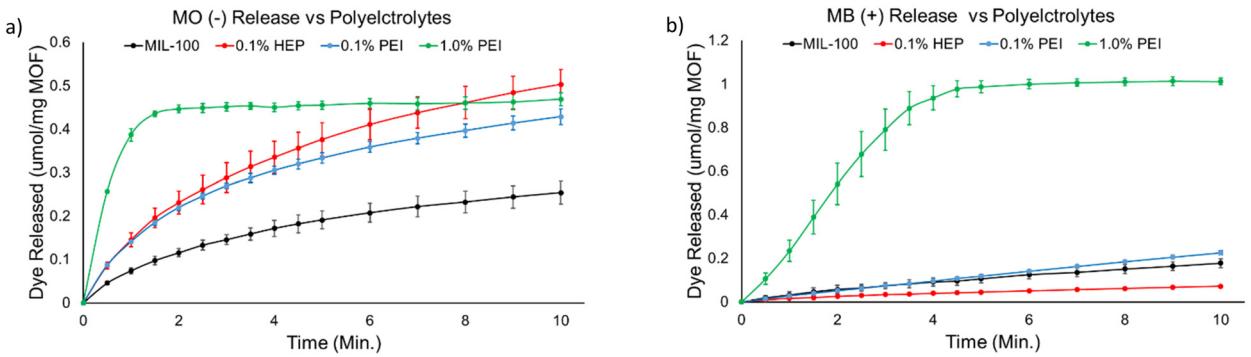

Fig. 7 Release plots obtained depicting the effect of polyelectrolytes on the release of negatively charged MO (a) and positively charged MB (b) from MIL-100. Data are shown as mean ± standard error of the mean (n = 3).

the HEP appears to coat the MOF preventing release, unlike in the MO trial. This is supported by the K–P values which indicate a slower release rate that is more hindered than the standard trial (k = 0.018, n = 0.66). Conversely, the 0.1% PEI trial sees an increase in release to 26.1%, with k dipping slightly compared to the standard with a value of 0.03 while n increased to 0.93. This increased and sustained release indicates that the PEI infiltrates the MOF pore and progressively kicks out MB over time.

After observing the increased release for both electrolytes with the addition of PEI, the concentration was increased to 1% to evaluate whether the release rate could be further improved. The HEP release at this concentration was not examined as the polyelectrolyte was more likely to interact with the framework rather than promote release at higher concentrations and had failed to promote release among both models. For this test, a burst release for MO was observed where 97.9% of the dye was released at 2 minutes indicating zero-order kinetics. It should be noted that much of the release occurred prior to UV-Vis measurement during the burst phase could not be observed. Analysing the release data with eqn (2) showed there was corresponding high k_1 of 2.037 with an accompanying n_1 of 1.26 while k_2 had a value of 0.035 with a n_2 of 1.00. These results indicate rapid assisted release of dye with an additional assisted release during diffusion, likely influenced by the Cl^- counter ions introduced in solution with the PEI in both cases.

When the PEI concentration is increased to 1%, there is a sustained zero-order release of dye until 3 minutes where the dye has completely been released. This is accompanied by a k value of 0.231 and a n of 1.19 indicating fast released influenced by the presence of the PEI. Under these conditions with other materials, the observed high n value would typically indicate that the surrounding structure is deteriorating, however, when the stability of the MOF was evaluated using PXRD there was no significant change in peak intensity or shape demonstrating the robustness of the MOF and its ability to withstand the inclusion of these charged polyelectrolytes (Fig. S29†). When combined with our earlier results, this data reveals that a restriction on release remains for MB as the burst release observed among the MO trial is absent. This is likely due to concentration gradients and continued congestion at the aforementioned pore window interface. Additionally, a selective component to release can be observed where molecules carrying either positive or negative charges may be released using positively charged polyelectrolytes while negatively charged polyelectrolytes primarily trigger the release of only negatively charged guests. Together, these results of dye release showcase how polyelectrolytes can be leveraged to control the release of drugs and the pitfall that some may encounter where coating of MOFs may lead to unintended premature release of loaded drug.

Polyelectrolyte assisted release of medically relevant drugs

Inspired by the positive results while testing the dye models, the efficacy of polyelectrolyte assisted release on drugs was then evaluated. Epinephrine (Ep) and Penicillin G (Pg), two drugs commonly found in medical procedures, were selected for analysis. The positively charged Ep and negatively charged Pg to be loaded and released from the MOF MIL-100. We utilized PEI to promote release as it had increased release irrespective of charge. These results mirrored that of the charged dyes with high release showing a direct relationship between PEI and release with a maximum release of 92.7% for Ep and 87.8% for Pg after 10 minutes (Fig. S30†).

Next, we tested the release efficacy of Ep in the presence of human mesenchymal stem cells (hMSCs) and performed quantitative evaluation using PrestoBlue™ (Fig. 8). During this test, we utilized the optimized conditions of 1% PEI for release and compared that to two control groups of MOFs alone and Ep loaded MOF of the same concentration with 0.1% PEI in solution. The effect of Pg was not tested as it would likely have no observable changes.

Cells cultured on tissue culture plastic (control) showed the highest viability, set as the reference (100%). MOFs without epinephrine exhibited a slight but non-significant decrease in cell viability, suggesting good biocompatibility of the MIL-100 (Fe) carrier. Notably, cells exposed to epinephrine released *via* MOFs in the presence of 0.1% PEI maintained comparable viability to the MOF-only group, indicating that low-dose epinephrine (~17 ng mL^{-1}) did not impair cellular health. While a moderate decrease in viability was observed at 1.0% PEI (~50 ng mL^{-1}), viability remained above 75% and only this group reached statistical significance compared to the control (p < 0.05). This is understood to be a result of increase metabolic activity due to the presence of Ep leading to slower cellular proliferation.[51]

To complement these findings, bright-field microscopy images were captured to evaluate cell morphology and adhesion patterns after three days of culture (Fig. S31†). In all groups, hMSCs preserved their typical elongated, spindle-like morphology and formed confluent monolayers. No clear mor-

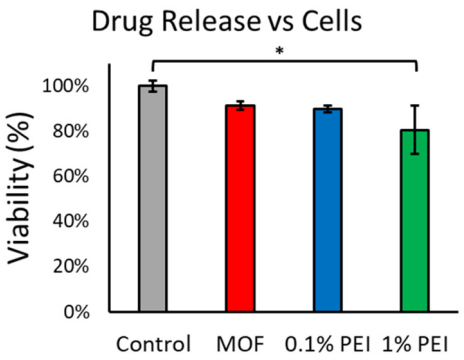

Fig. 8 Cell viability results following the release of epinephrine from MIL-100, measured using the PrestoBlueTM HS assay. Results are expressed as percentage of the TCP control group (set at 100%). A statistically significant decrease in viability was observed only in the 1.0% PEI condition (p < 0.05). Results are shown as mean ± standard error of the mean (n = 5).

phological abnormalities or signs of cytotoxicity, such as cell rounding, detachment, or fragmentation, were observed. Even in the 1.0% PEI group, cells retained their structural characteristics, though a slightly reduced density was noticeable, consistent with the lower viability detected in the fluorescence assay.

Conclusion

The delivery of drugs, whether by targeting or non-specific release, is an important avenue of research that can have life-saving effects. The selection of appropriate combinations of linkers, metal centres, and associated materials, like coatings and targeting moieties, create environments within and surrounding MOFs that can have significant implications on drug loading and release. Here, the effects of electrostatic interactions across a range of conditions are probed utilizing charged dye and drugs models. Our findings highlight the interactions between these molecules, the surrounding MOF, and other electrostatic groups like ions and polyelectrolytes during release and provide new insight these interactions which can be leveraged in the administration of charged drug molecules from MOFs.

We also introduced a novel mathematical model adapted from the Korsmeyer–Peppas model that allowed for the appropriate modelling of biphasic burst release and the subsequent diffusion driven release of loaded molecules from within MOFs. Using these two models allowed empirical insights to be extracted from the results which showed how factors like loading, presence of electrostatic functional groups, buffer concentration, and the presence of polyelectrolytes can influence drug release. Finally, these findings were tested using drug models and human mesenchymal stem cells to determine efficacy with satisfactory results. Together, the findings from this work can inform the decisions of researchers and enable them to avoid pitfalls by highlighting how conditions and electrostatic interactions can influence and be leveraged to create a ubiquitous platform for controlled drug delivery. This broad approach can effectively bypass the boutique approach where the selection of specific linkers and coatings which can become cost prohibitive for widespread implementation of MOFs for medicinal use.

Author contributions

J. P. and S. M. was responsible for conceptualization, methodology, data curation, and project administration; formal analysis was conducted by J. P., L. P.-H., J. A., and S. M.; funding acquisition was carried out by J. A., T. A., and S. M., investigation was carried out by J. P., L. P.-H., W. F., S. N., P. W., A. T., and T. B.; supervision was conducted by J. A. and S. M.; J. P., L. P.-H., W. F., S. N., P. W., A. T., and T. B. were responsible for writing – original draft; J. P., L. P.-H., J. A., and S. M. were responsible for writing – review & editing.

Data availability

The data that support the findings of this study are available from the corresponding author upon reasonable request. This includes raw and processed data generated during the current study. Any additional data or materials required for replication of the results can also be provided by the corresponding author.

Conflicts of interest

The authors declare no conflicts of interest.

Acknowledgements

The authors acknowledge the financial support from the Robert A. Welch Foundation (B-0027) for this work. Partial support from Princess Nourah bint Abdulrahman University Researchers Supporting Project number (PNURSP2025R1), Riyadh, Saudi Arabia (T. A.) is also acknowledged.

References

1 R. Freund, O. Zaremba, G. Arnauts, R. Ameloot, G. Skorupskii, M. Dincă, A. Bavykina, J. Gascon, A. Ejsmont, J. Goscianska, M. Kalmutzki, U. Lächelt, E. Ploetz, C. S. Diercks and S. Wuttke, *Angew. Chem., Int. Ed.*, 2021, **60**, 23975–24001.
2 S. Ma and H.-C. Zhou, *Chem. Commun.*, 2010, **46**, 44–53.
3 M. Carboni, C. W. Abney, S. Liu and W. Lin, *Chem. Sci.*, 2013, **4**, 2396–2402.
4 L. Jiao, Y. Wang, H.-L. Jiang and Q. Xu, *Adv. Mater.*, 2018, **30**, 1703663.
5 J. Phipps, H. Chen, C. Donovan, D. Dominguez, S. Morgan, B. Weidman, C. Fan and H. Beyzavi, *ACS Appl. Mater. Interfaces*, 2020, **12**, 26084–26094.
6 Y. Du, X. Jia, L. Zhong, Y. Jiao, Z. Zhang, Z. Wang, Y. Feng, M. Bilal, J. Cui and S. Jia, *Coord. Chem. Rev.*, 2022, **454**, 214327.
7 C. Fu, T. Lu, X. Dai, P. Ding, Y. Xiong, J. Ge and X. Li, *ACS Appl. Mater. Interfaces*, 2023, **15**, 6859–6867.
8 V. Lykourinou, Y. Chen, X.-S. Wang, L. Meng, T. Hoang, L.-J. Ming, R. L. Musselman and S. Ma, *J. Am. Chem. Soc.*, 2011, **133**, 10382–10385.
9 F.-S. Liao, W.-S. Lo, Y.-S. Hsu, C.-C. Wu, S.-C. Wang, F.-K. Shieh, J. V. Morabito, L.-Y. Chou, K. C.-W. Wu and C.-K. Tsung, *J. Am. Chem. Soc.*, 2017, **139**, 6530–6533.
10 F.-K. Shieh, S.-C. Wang, C.-I. Yen, C.-C. Wu, S. Dutta, L.-Y. Chou, J. V. Morabito, P. Hu, M.-H. Hsu, K. C.-W. Wu and C.-K. Tsung, *J. Am. Chem. Soc.*, 2015, **137**, 4276–4279.
11 H. Sun, Y. Li, S. Yu and J. Liu, *Nano Today*, 2020, **35**, 100985.
12 F. Lyu, Y. Zhang, R. N. Zare, J. Ge and Z. Liu, *Nano Lett.*, 2014, **14**, 5761–5765.
13 X. Wu, H. Yue, Y. Zhang, X. Gao, X. Li, L. Wang, Y. Cao, M. Hou, H. An, L. Zhang, S. Li, J. Ma, H. Lin, Y. Fu, H. Gu,

W. Lou, W. Wei, R. N. Zare and J. Ge, *Nat. Commun.*, 2019, **10**, 5165.
14 X. Ge, F. Jiang, M. Wang, M. Chen, Y. Li, J. Phipps, J. Cai, J. Xie, J. Ong, V. Dubovoy, J. G. Masters, L. Pan and S. Ma, *ACS Appl. Mater. Interfaces*, 2023, **15**, 677–683.
15 Y. Feng, H. Wang, S. Zhang, Y. Zhao, J. Gao, Y. Zheng, P. Zhao, Z. Zhang, M. J. Zaworotko, P. Cheng, S. Ma and Y. Chen, *Adv. Mater.*, 2019, **31**, 1805148.
16 Y. Chen, S. Hong, C.-W. Fu, T. Hoang, X. Li, V. Valencia, Z. Zhang, J. A. Perman and S. Ma, *ACS Appl. Mater. Interfaces*, 2017, **9**, 10874–10881.
17 X. Chen, R. Tong, Z. Shi, B. Yang, H. Liu, S. Ding, X. Wang, Q. Lei, J. Wu and W. Fang, *ACS Appl. Mater. Interfaces*, 2018, **10**, 2328–2337.
18 Q. Sun, X. Hou, J. Yang, M. Zhang, Y. Yang, Y. Liu, W. Shen and D. Yin, *ACS Appl. Mater. Interfaces*, 2021, **13**, 55577–55590.
19 J. Gandara-Loe, B. E. Souza, A. Missyul, G. Giraldo, J.-C. Tan and J. Silvestre-Albero, *ACS Appl. Mater. Interfaces*, 2020, **12**, 30189–30197.
20 Y.-H. Hong, M. Narwane, L. Y.-M. Liu, Y.-D. Huang, C.-W. Chung, Y.-H. Chen, B.-W. Liao, Y.-H. Chang, C.-R. Wu, H.-C. Huang, I.-J. Hsu, L.-Y. Cheng, L.-Y. Wu, Y.-L. Chueh, Y. Chen, C.-H. Lin and T.-T. Lu, *ACS Appl. Mater. Interfaces*, 2022, **14**, 3849–3863.
21 B. Liu, Z. Liu, X. Lu, P. Wu, Z. Sun, H. Chu and H. Peng, *Mater. Des.*, 2023, **228**, 111861.
22 P. Jing, M. Wu, J. Su, L. Zhang, X. Cao and K. Jiang, *Mater. Lett.*, 2023, **349**, 134812.
23 M. He, J. Zhou, J. Chen, F. Zheng, D. Wang, R. Shi, Z. Guo, H. Wang and Q. Chen, *J. Mater. Chem. B*, 2015, **3**, 9033–9042.
24 C.-Y. Sun, C. Qin, X.-L. Wang, G.-S. Yang, K.-Z. Shao, Y.-Q. Lan, Z.-M. Su, P. Huang, C.-G. Wang and E.-B. Wang, *Dalton Trans.*, 2012, **41**, 6906–6909.
25 H. Zheng, Y. Zhang, L. Liu, W. Wan, P. Guo, A. M. Nyström and X. Zou, *J. Am. Chem. Soc.*, 2016, **138**, 962–968.
26 K. Suresh and A. J. Matzger, *Angew. Chem., Int. Ed.*, 2019, **58**, 16790–16794.
27 X. Du, R. Fan, L. Qiang, K. Xing, H. Ye, X. Ran, Y. Song, P. Wang and Y. Yang, *ACS Appl. Mater. Interfaces*, 2017, **9**, 28939–28948.
28 J. Salazar, Y. Hidalgo-Rosa, P. C. Burboa, Y. Wu, N. Escalona, A. Leiva, X. Zarate and E. Schott, *J. Controlled Release*, 2024, **370**, 392–404.
29 Z. Li, Y. Peng, X. Xia, Z. Cao, Y. Deng and B. Tang, *Sci. Rep.*, 2019, **9**, 17570.
30 M. Lalinia, N. H. Nemati, P. Mofazali, J. D. Gross and A. Samadi, *Mater. Today Chem.*, 2025, **45**, 102640.
31 Z. Dong, Y. Sun, J. Chu, X. Zhang and H. Deng, *J. Am. Chem. Soc.*, 2017, **139**, 14209–14216.
32 N. Pederneira, K. Newport, S. Lawson, A. A. Rownaghi and F. Rezaei, *ACS Appl. Bio Mater.*, 2023, **6**, 2477–2486.
33 B. E. Souza, L. Donà, K. Titov, P. Bruzzese, Z. Zeng, Y. Zhang, A. S. Babal, A. F. Möslein, M. D. Frogley, M. Wolna, G. Cinque, B. Civalleri and J.-C. Tan, *ACS Appl. Mater. Interfaces*, 2020, **12**, 5147–5156.
34 P. Horcajada, C. Serre, M. Vallet-Regí, M. Sebban, F. Taulelle and G. Férey, *Angew. Chem., Int. Ed.*, 2006, **45**, 5974–5978.
35 J. Gordon, H. Kazemian and S. Rohani, *Mater. Sci. Eng., C*, 2015, **47**, 172–179.
36 Y. Sun, L. Zheng, Y. Yang, X. Qian, T. Fu, X. Li, Z. Yang, H. Yan, C. Cui and W. Tan, *Nano-Micro Lett.*, 2020, **12**, 103.
37 Z. Zong, G. Tian, J. Wang, C. Fan, F. Yang and F. Guo, *Pharmaceutics*, 2022, **14**, 2790.
38 P. L. Ritger and N. A. Peppas, *J. Controlled Release*, 1987, **5**, 23–36.
39 L. Hoellein and U. Holzgrabe, *Int. J. Pharm.*, 2012, **434**, 468–480.
40 C. N. Banti, I. Ketikidis, S. K. Hadjikakou, A. G. Hatzidimitriou, A. M. Grześkiewicz, M. Kubicki and N. Hadjiliadis, *Inorg. Chim. Acta*, 2020, **509**, 119683.
41 T. He, X. Xu, B. Ni, H. Wang, Y. Long, W. Hu and X. Wang, *Nanoscale*, 2017, **9**, 19209–19215.
42 F. Zhang, J. Shi, Y. Jin, Y. Fu, Y. Zhong and W. Zhu, *Chem. Eng. J.*, 2015, **259**, 183–190.
43 T. Simon-Yarza, T. Baati, F. Neffati, L. Njim, P. Couvreur, C. Serre, R. Gref, M. F. Najjar, A. Zakhama and P. Horcajada, *Int. J. Pharm.*, 2016, **511**, 1042–1047.
44 G. Zhong, D. Liu and J. Zhang, *Cryst. Growth Des.*, 2018, **18**, 7730–7744.
45 C. Serre, S. Bourrelly, A. Vimont, N. A. Ramsahye, G. Maurin, P. L. Llewellyn, M. Daturi, Y. Filinchuk, O. Leynaud, P. Barnes and G. Férey, *Adv. Mater.*, 2007, **19**, 2246–2251.
46 H. Leclerc, T. Devic, S. Devautour-Vinot, P. Bazin, N. Audebrand, G. Férey, M. Daturi, A. Vimont and G. Clet, *J. Phys. Chem. C*, 2011, **115**, 19828–19840.
47 R. W. Korsmeyer, R. Gurny, E. Doelker, P. Buri and N. A. Peppas, *Int. J. Pharm.*, 1983, **15**, 25–35.
48 P. Trucillo, *Processes*, 2022, **10**, 1094.
49 S. Dash, P. N. Murthy, L. Nath and P. Chowdhury, *Acta Pol. Pharm.*, 2010, **67**, 217–223.
50 J. An, S. J. Geib and N. L. Rosi, *J. Am. Chem. Soc.*, 2009, **131**, 8376–8377.
51 R. Zhang, B. Yao, R. Li, S. W. Limesand, Y. Zhao and X. Chen, *Int. J. Mol. Sci.*, 2024, **25**, 7029.